Volume 1 | Number 1 | Jan 2013 | Pages 1–100

Dalton Transactions

An international journal of inorganic chemistry
www.rsc.org/dalton

ROYAL SOCIETY OF CHEMISTRY

This is an *Accepted Manuscript*, which has been through the Royal Society of Chemistry peer review process and has been accepted for publication.

Accepted Manuscripts are published online shortly after acceptance, before technical editing, formatting and proof reading. Using this free service, authors can make their results available to the community, in citable form, before we publish the edited article. We will replace this *Accepted Manuscript* with the edited and formatted *Advance Article* as soon as it is available.

You can find more information about *Accepted Manuscripts* in the **Information for Authors**.

Please note that technical editing may introduce minor changes to the text and/or graphics, which may alter content. The journal's standard **Terms & Conditions** and the **Ethical guidelines** still apply. In no event shall the Royal Society of Chemistry be held responsible for any errors or omissions in this *Accepted Manuscript* or any consequences arising from the use of any information it contains.

Dalton Transactions

Journal Name

ARTICLE

Surface Confinement of TbPc$_2$-SMMs: Structural, Electronic and Magnetic Properties

Eufemio Moreno Pineda,[a] Tadahiro Komeda,[b] Keiichi Katoh,[c] Masahiro Yamashita[c,d] and Mario Ruben[a,d,e*]
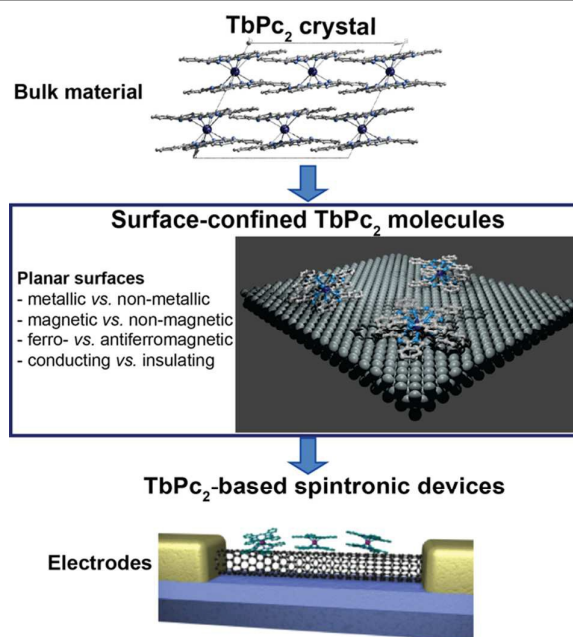
Since 2003 terbium(III) *bis*-phthalocyaninato complexes have been recognised to act as single molecule magnets (SMMs), propitiating multiple studies with the aim of better understanding of the single metal-ion based magnetism with unusually high blocking temperatures. In the quest of novel applications, it became clear that if spintronic devices were made from SMM molecules, their confinement in the proximity of surfaces or electrodes would become difficult to circumvent. In this perspective article we highlight the influence of the presence of different substrates onto the magnetic performance of TbPc$_2$-SMMs; in principle caused, among other effects, by electronic hybridization, dipole-dipole coupling, and by changing quantum tunnelling (QT) rates once on surface. We show that the improved comprehension of how SMMs interact and communicate with the environment finally leads to magnetic remanence and lower tunnelling rates, paving the way to novel classes of spintronic devices.

Introduction

Molecular spintronic sets a new scenario for the technology industry, where current materials are approaching molecular levels. Molecules offer the advantage of being prepared in a wide range of combinations, the products having the exact characteristics of the others. Many molecular systems have been proposed as candidates for molecular spintronics, however, amongst them single molecule magnets (SMMs) show promising properties to act as elementary units given that these molecules exhibit magnetic hysteresis purely at molecular level.[1]

Broadly speaking the SMM family can be classified into transition metal- and lanthanide-containing systems, being the latter more attractive for technological applications due to blocking of the magnetisation at single ion level.[2] The first observation of such behaviour in lanthanide-based molecules was achieved in double decker lanthanide phthalocyanine complexes, seminal work reported by Ishikawa and co-workers in 2003.[2] Since then, many other lanthanide-based SMMs have

been reported[3] with wider hysteretic loops and energy barriers up to two orders of magnitude higher than the observed in the 3d-counterparts.[3,4] Obviously, the subsequent unavoidable step towards the implementation of SMMs in molecular-based magneto-electronic devices is directly associated with their confinement onto surfaces (Fig. 1).[5]

Figure 1. From the bulk to the spintronic devices: The pivotal role of surface confinement in the exploitation of the magnetic properties of Terbium (III) bis-phthalocyaninato (TbPc$_2$) single molecule magnets.
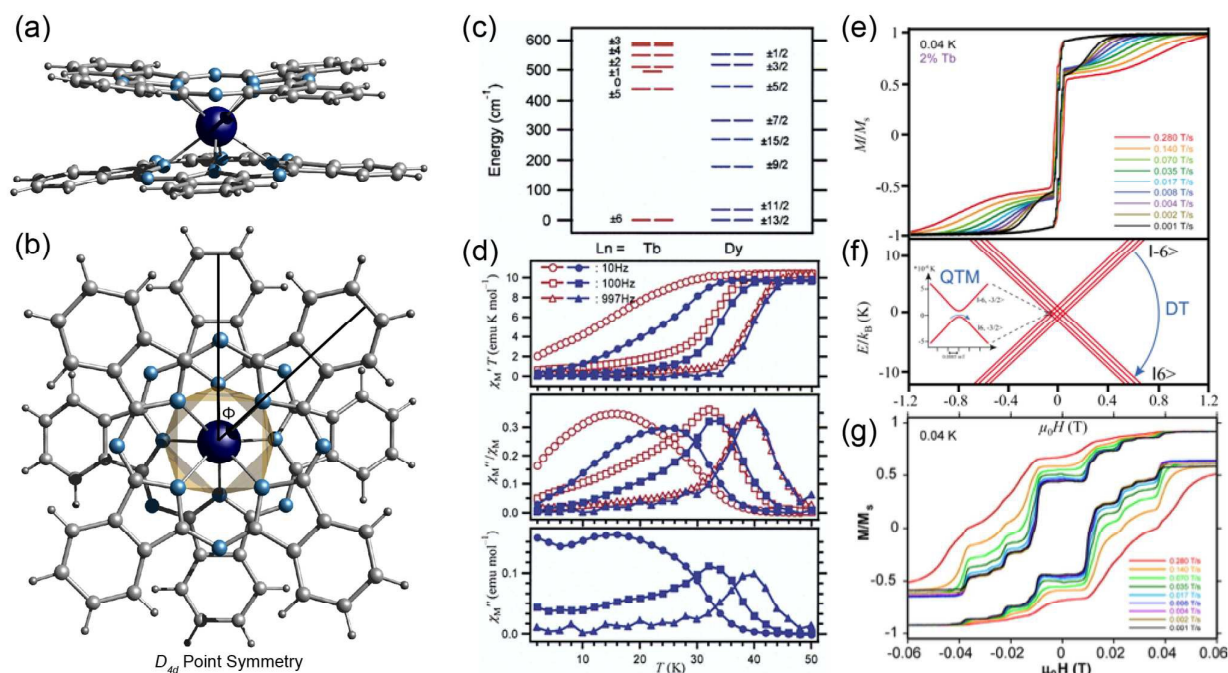
a. *Institute of Nanotechnology (INT), Karlsruhe Institute of Technology (KIT), Hermann-von-Helmholtz-Platz 1, D-76344 Eggenstein-Leopoldshafen, Germany. E-mail Mario.Ruben@kit.edu*
b. *Institute of Multidisciplinary Research for Advanced Materials (IMRAM, Tagen) Tohoku University*
c. *Department of Chemistry, Graduate School of Science, Tohoku University, Aramaki-Aza-Aoba, Aoba-Ku, Sendai 980-8578, Japan. E-mail: yamasita@agnus.chem.tohoku.ac.jp*
d. *WPI Research Center, Advanced Institute for Materials Research, Tohoku University, 2-1-1 Katahira, Aoba-ku, Sendai 980-8577, Japan*
e. *Institut de Physique et Chimie des Matériaux de Strasbourg (IPCMS), CNRS-Université de Strasbourg, 23 rue du Loess, BP 43, F-67034 Strasbourg Cedex 2, France*

ARTICLE Journal Name

Figure 2. Crystal structure of [TbPc$_2$]$^{\pm/0}$ (a) side and (b) top view. Panel b shows the polyhedral representation of the TbN$_8$ coordination environment with D_{4d}-square-antiprismatic coordination geometry. Colour code: H, dark grey; C, grey; N, cyan; Tb, dark blue. The TBA counter ion was omitted for clarity. (c) Energy diagram for TBA[LnPc$_2$] (Ln = Tb^{3+} and Dy^{3+}) determined by Ishikawa (note the large separation between ground and first exited state for Tb^{+3}) and (d) Dynamic magnetic behaviour of TBA[TbPc$_2$] neat sample (open symbols) and diluted into TBA[YPc$_2$] (filled symbols), at zero DC field and an oscillating field of 3.5 G at varied frequencies. (e) Reported hysteresis loops for a single crystal of diluted TBA[Tb$_{0.02}$Y$_{0.98}$Pc$_2$] at different scan rates collected at T = 40 mK with the field applied along the easy axes of the magnetisation. (f) Schematic representation of the split magnetic ground state J = 6 into four states by hyperfine interaction with the nuclear spin I = $^3/_2$ with quantum tunnelling of magnetisation (QTM) al low fields and direct tunnelling (DT) at higher fields as the two dominating tunnelling mechanisms. (g) Zoom in into the region around zero field exhibiting steps due to the QTM. Adapted with permission from ref. 2.

Contrary to fact, however just few of the many SMM candidates have been successfully deposited on surfaces, mainly due to their chemical instability[6] and their lack of physical integrity once deposited on surfaces. Interestingly, the lanthanide phthalocyanine complexes continue to play a key role in the molecular spintronic research due to their extraordinary robustness. More precisely, the uncharged TbPc$_2$ complex has been extensively studied for its neutral characteristics which allows its sublimation on a wide range of surfaces (*vide infra*).

For a successful implementation of these molecular units in devices, a thorough understanding must be achieved. In this regard, the bulk magnetic properties of lanthanide SMMs have been probed by an extensive range of spectroscopic[7] and magnetic techniques,[8] affording reasonable understanding of the bulk magnetic properties. Conversely, deposition of SMMs on surfaces represents a totally new challenge, given that although reducing intermolecular interactions and crystal packing effects, on-surface-SMM behaviour can cause distortion of the crystal field around the metal centre(s) leading to different magnetic behaviours up to total quenching of the magnetic properties. Moreover, surface-molecule contact can introduce further interactions, that need to be understood for a successful application in hybrid molecular devices, e.g. factor affecting the quantum tunnelling of the magnetisation and hysteresis loops at surface level.

It is the scope of this perspective article to present the reader with an overview of the physical and magnetic properties of the very well-known TbPc$_2$ on different

substrates, showing more precisely how surface-TbPc$_2$ interactions can affect the magnetic hysteresis as well as some insight into the understanding of TbPc$_2$-surface behaviour hitherto gained.

Structure and Bulk Magnetism of [TbPc$_2$]$^{\pm,0}$

Before proceeding with our account, a brief description of the magnetic and structural characteristics of [TbPc$_2$]$^{\pm,0}$ will be given. Along with the well-known {Mn$_{12}$}[9] and {Fe$_4$}[6a,b] complexes, [TbPc$_2$]$^{\pm,0}$ stands as one of the most studied SMM. The discovery of the energy barrier to the relaxation of the magnetisation (U_{eff}), at single ion level, in the TBA[LnPc$_2$] complex (TBA = tetrabutylammonium and Ln = Tb^{3+} and Dy^{3+}) was realised by Ishikawa et al in 2003.[2a] Interestingly, the terbium analogue showed the most astonishing properties.

Structurally, [TbPc$_2$]$^-$ features a central Tb^{3+} octa-coordinated ion sandwiched between two parallel aligned phthalocyanines, with a skew angle between the Pc-ligands close to 45°, leading to a square-antiprismatic (D_{4d}) coordination geometry (Fig. 2a,b). NMR and SQUID studies conducted by Ishikawa and co-workers showed a large energy separation ca. 600 K of the ground state and the first excited state for the Tb^{3+} analogue (Fig. 2c).[2b] The low-lying electronic structure of the TBA[TbPc$_2$] indicated a highly axial ground state with m$_J$ = ±6, the maximum possible for Tb^{3+} ion (^{7}F$_6$). Posteriorly, alternating-current (AC) magnetic susceptibility measurements revealed a frequency dependence of the magnetic behaviour, characteristic of SMMs. The magnetic

features of TBA[TbPc$_2$] showed an out-of-phase maximum in the $\chi''(T)$ at 40 K (1 kHz), later corroborated by studies of the magnetically diluted material (Fig. 2d), where intermolecular effects are reduced, revealing solely the molecular magnetic properties.[2a] Moreover, the authors reported the observation of magnetic hysteresis in diluted samples at 1.7 K,[2c] later confirmed by μ-SQUID studies. Interestingly, μ-SQUID data showed not just the butterfly-shaped hysteretic curves but also quantum tunnelling steps triggered by the hyperfine interaction between the m_J states (±6) of the Tb^{3+} ion with the nuclear spin ($I = {}^3/_2$) (Fig. 2e-g).[2e]

Furthermore, it has been shown that it is also possible to modify the crystal field of the negative complex by either oxidation which leads to the neutral TbPc$_2$, with an improved U_{eff} associated with a π-radical ($S = \frac{1}{2}$) delocalised over the Pc ligands and the $J = 6$ ground state of the Tb^{3+} ion, or enhancement by peripheral substitution of Pc groups or oxidation.[10]

The neutral TbPc$_2$ analogue is the subject of this perspective article, given that it can be deposited on surfaces employing a variety of deposition techniques, allowing extensive studies by the research community.

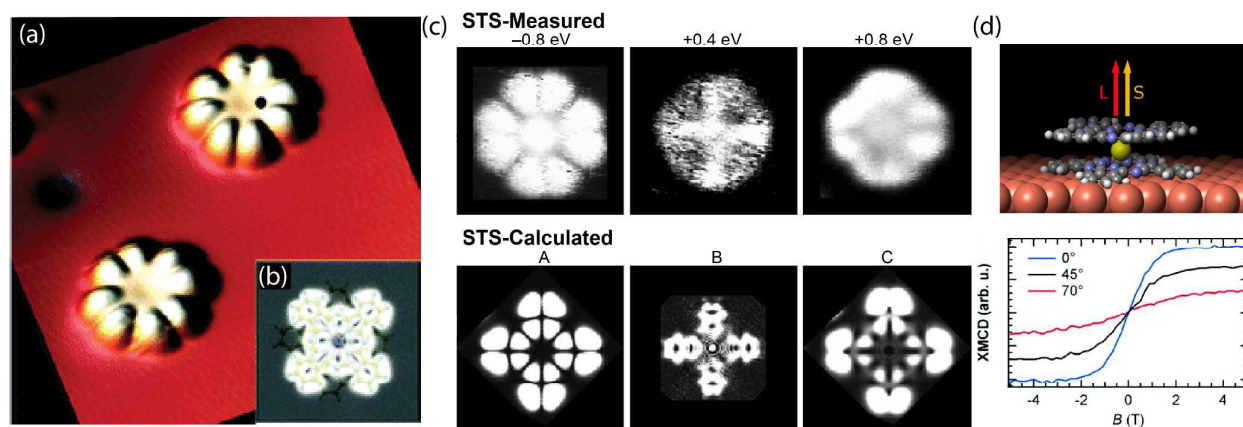## Deposition of TbPc$_2$ on Non-Magnetic Metallic Substrates

Deposition of TbPc$_2$ on a number of substrates has been achieved since it withstands vacuums and temperature conditions needed for sublimation of clean, uniform monolayers, without affecting its structural nature. In the following sections the structural and magnetic properties of TbPc$_2$ deposited on metallic non-magnetic surfaces will be surveyed with the goal of identifying the boundary conditions favourable for the constitution of molecular spintronic devices.

The structural integrity of the neutral TbPc$_2$ was firstly described in 2008 by Vitali et al. after depositing the molecule onto Cu(111) surface at ultrahigh vacuum (UHV), employing a dry-imprinting technique.[11] Discrete molecules and aggregates were obtained. The sample was characterised via Scanning Tunnelling Microscopy (STM) at 10 K. Analysis of the STM

topographic images and conductance maps of an isolated TbPc$_2$ molecule onto the Cu(111) surface showed that the molecule lays flat on the Cu(111) surface, being totally independent of the hexagonal lattice of the substrate. Two phthalocyanines were distinguished with a skew angle θ ~ 45° leading to an 8-fold symmetry pattern, in agreement with the crystal structure of the TbPc$_2$.[2] The height of the TbPc$_2$ on the surface showed to be close to 3 Å, as observed for the Pc···Pc height on bulk (Fig. 3).

The results clearly indicated that the TbPc$_2$ molecule was very robust, withstanding ultrahigh vacuums; however a major question emerged after the confirmation of the structural integrity of TbPc$_2$ on Cu(111) and it was whether surface-molecule interactions could hinder, preclude, or even improve its magnetic properties. Vitali and co-workers addressed this question through Scanning Tunnelling Spectroscopy (STS) studies along with Density Functional Theory (DFT). Qualitative insight into the electronic and magnetic properties of the system was gained after comparison of: (*i*) the dI/dV spectrum of the on-surface TbPc$_2$, where two major peaks were present, (*ii*) the calculated dI/dV spectrum of an isolated neutral TbPc$_2$, (*iii*) an isolated negatively charged [TbPc$_2$]$^-$ and (*iv*) a fictitious TbPc$_2$ deposited on Cu(111). Analysis of the experimentally determined electronic states of the deposited neutral compound showed that on Cu(111) the anionic system ([TbPc$_2$]$^-$) was formed. Moreover, the spin-resolved electronic states of a model TbPc$_2$ deposited on a Cu(111) surface, assuming very strong surface-molecule interactions, were computed. The strong interaction showed hybridization of the delocalised unpaired electron of the ligands and the surface, suppressing the radical character of the ligands, but showing no net effect on the large magnetic moment of the Tb^{3+}. Comparison of the experimental energy resolved conductance maps of the TbPc$_2$ on Cu(111) with the computed maps of [TbPc$_2$]$^-$ supported this picture (Fig. 3b,c). Remarkably, albeit the strong hybridization, no effect on the magnetism of the 4f states of the Tb^{3+} ion was observed.

Further proofs of the magnetic properties of the on-surface TbPc$_2$ were later provided by Stepanow and co-workers, through the element sensitive X-ray Magnetic Circular
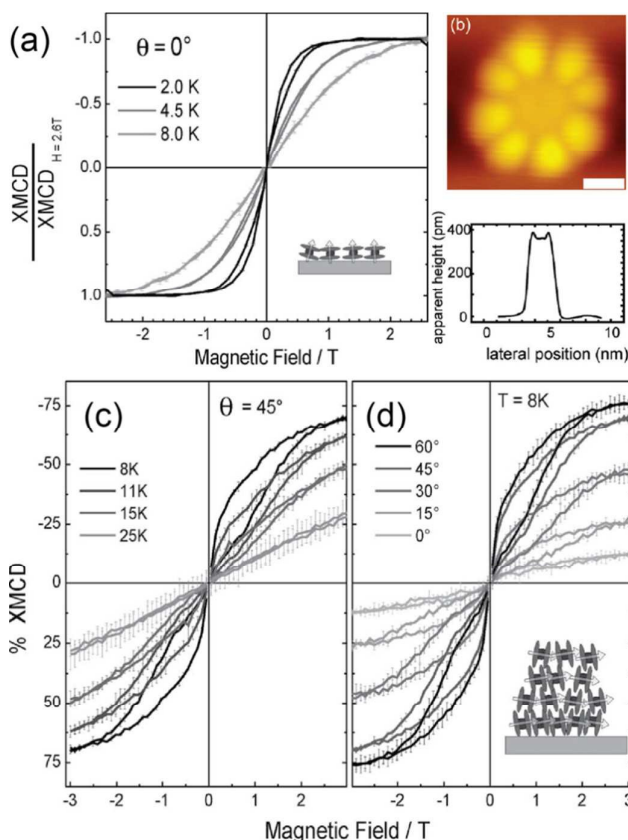

Figure 3. (a) Topographic image at constant current of two isolated TbPc$_2$ molecules on Cu(111) surface. (b) STM simulation image of isolated TbPc$_2$ molecule. (c) Experimental (top) and calculated (bottom) energy-resolved charge densities. (d) Schematic representation of TbPc$_2$ on Cu(111) with the spin (S) and angular momentum (L) (top) Magnetisation curves obtained from the Tb M_5 XMCD intensity for TbPc$_2$ on Cu(100) at T = 8 K (bottom). Adapted with permission from ref. 11 and 13.

Dichroism (XMCD)[12] on isolated $TbPc_2$ deposited on Cu(100).[13] For this study Cu(100) was chosen due to its strong molecule substrate interactions, which prevents the formation of agglomerates, commonly observed in Cu(111).[14] XMCD measurements allowed the determination of the orbital and spin magnetic moments separately, therefore yielding direct access to the anisotropic behaviour of $TbPc_2$. The data acquisition of the X-ray absorption spectra (XAS) at the terbium edge ($M_{4,5}$) comprised the temperature range between 300 and 8 K, in magnetic field up to 5 T, using right (I^+) and left (I^-) circularly polarised light. Excellent agreement between the XAS line shape of the theoretical Tb^{+3} $4f^8$ configuration (with $J = 6$ ground state, $L = 3$; $S = 3$) and the experimental data was found. Moreover, the XMCD ($I^- - I^+$) intensity at 8 K and 5 T along with the $M_{4,5}$ XMCD branching ratio suggested the presence of a large orbital moment, as expected for Tb^{3+}. These experiments revealed the strong Ising-like properties of the surface-confined $TbPc_2$, suggesting the full spin magnetic moment expected for a $J = 6$ ground state along the easy axis and vanishing magnetisation in the hard Pc plane (Fig. 3d). X-ray natural linear dichroism (XNLD) measurements also confirmed the flat orientation of the molecules on the surface, pinpointing that the molecules were highly oriented and the 4f shell was subjected to strong crystal field effects (Fig. 3d). In this study, despite the strong anisotropic character of the on-surface molecule, no magnetic hysteresis down to 8 K was detected.[13] This fact was attributed to the measurement timescale being up to 7 orders of magnitude larger than in measurements based on AC susceptibility.

As earlier described, $TbPc_2$ can be successfully deposited onto Cu(100), preserving both, the structural integrity and the magnetic properties associated to the Tb^{3+} ion. Despite this however, no hysteresis was observed, important requirement for data storage applications, and quantum computing.[15] In the quest of such property Margheriti et al. explored the magnetic behaviour of the $TbPc_2$ employing XMCD technique.[16] The studies were conducted on a thick film of $TbPc_2$ deposited on aluminium foil, under UHV conditions. Thin films were also prepared, depositing $TbPc_2$ onto an Au(111) substrate. The on-surface samples were characterised using time-of-flight secondary ion mass spectrometry (Tof-SIMS), corroborating that $TbPc_2$ was intact on the surface. A strong dichroic signal was found in $TbPc_2$(200 nm)/Al sample in the XNLD measurements, highlighting a preferential orientation of the $TbPc_2$ on the films. The authors determined that $TbPc_2$ was arranged in a flat configuration when deposited onto Au(111) (as thin film) (Fig. 4b and inset Fig. 4a), whilst when deposited on Al foil (as thick film) the magnetic axes of the $TbPc_2$ were arranged in perpendicular fashion (standing configuration) (inset Fig. 4d).

The intensity of the XMCD spectra of the thick film confirmed the XNLD results, the molecules on the Al surface were organised in standing configuration. Conversely, the XMCD of the thin film confirmed that $TbPc_2$ lays flat on the surface. Comparing the normalised XMCD intensity of thick and thin films at θ = 45° it could be seen that in the thick film a

number of $TbPc_2$ maintain the hard axes parallel to the magnetic field.

Figure 4. (a) XMCD data for a $TbPc_2$ monolayer on Au(111) (thin film). (b) (top) STM topographic image and (bottom) cross-sectional view of $TbPc_2$ deposited on Au(11). (c) XMCD hysteresis loops of $TbPc_2$ deposited of Al foil (think film). Insets in panels a and d represent the orientation of $TbPc_2$ molecules and their easy axes of magnetisation in the films. from ref. 16 and 17.

Element sensitive hysteresis loops were posteriorly collected on thin and thick samples. $TbPc_2$ deposited on Al showed the most interesting magnetic behaviour; therefore, the temperature dependence was further studied revealing butterfly-like hysteresis loops, featuring strong quantum tunnelling near zero field (Fig. 4c,d), with blocking temperature higher than observed on bulk sample. On the contrary, the thin film showed no measurable hysteresis loops under similar conditions. Experiments realised using lower temperatures revealed just a very small opening of the loops on the thin film. (Fig. 4a).

The authors hypothesised that the differences of the hystereses loops could be attributed to surface-molecule interactions. It can certainly be seen that stronger surface-$TbPc_2$ interactions could be expected when the molecule lays flat on the surface, compared with the standing configuration observed when deposited on Al foil. Contrary to the Cu(100) case (8 K), a small opening of the hysteresis loop is observed when $TbPc_2$ is deposited on Au(111) at 2 K. Despite this, comparison of the surface-molecule interaction strength of Cu(100) and Au(111) cannot be established, due to the different temperatures employed during the XMCD data collection.

Additionally, LnPc$_2$ analogues (Ln = Y^{3+}, Dy^{3+} and Tb^{3+}) have been successfully deposited on Au(111) by Katoh et al., where they studied their physical properties and their possible applicability as Field Effect Transistors (FET).[17] In the study, the deposition of the LnPc$_2$ on Au(111) was achieved by sublimation of the pure material heated at 600 K on the Au(111) substrate. Contrary to the results obtained on the Cu(111) surface,[11] STM topographic images revealed two types of molecules with four- and eight-lobed motifs, in a MPc$_2$/MPc ratio of 4:1. The Pc ligands were found to be parallel to the normal of the Au(111) surface. The eight lobes pattern was consistent with the observed of TbPc$_2$ on copper surfaces, whilst the four-lobes structures were assigned to LnPc bricks, which have lost one Pc-ligand. This result shows that during the deposition via sublimation careful temperature conditions of both TbPc$_2$ sample and substrate is of utmost importance to guarantee integrity of the TbPc$_2$ molecules.[18] Nevertheless, alternative deposition techniques as electro spray deposition or brush stamping have proven that decomposition of TbPc$_2$ SMMs can be completely avoided on metallic surfaces, leading to even large extended monolayer assemblies.[11,14]

Remarkably, further studies of TbPc$_2$ on Au(111) by Komeda et al. showed the controlled manipulation of the Kondo peak, associated to $S = \frac{1}{2}$ delocalised over the Pc ligands, through systematic rotation of the Pc groups.[19] In a similar approach Fu et al. demonstrated that upon STM manipulation of a TbPc$_2$ deposited on Ir(111) sample the chirality of the molecule can be directly addressed,[20] both schemes highlighting the possibility of the implementation of TbPc$_2$ in information coding at molecular level.

Deposition of TbPc$_2$ on Magnetic Metallic Substrates

XMCD analysis of TbPc$_2$ deposited on Cu(100) showed no hysteresis, whilst hysteresis loops up to $T = 15$ K were observed in a multilayer TbPc$_2$ deposited on Al substrate, where the TbPc$_2$ organise in on-edge standing fashion. Studies of a monolayer of TbPc$_2$ however, exhibited a very shallow opening at $T = 2$ K, demonstrating that the magnetic moment was highly perturbed upon on-surface absorption.[13]
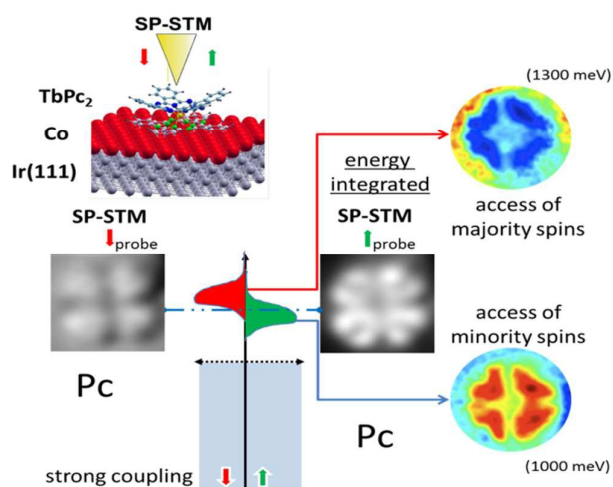
In this context, it has been proposed that deposition of TbPc$_2$ on magnetic metallic surfaces could help to stabilise the TbPc$_2$ magnetic moment, diminishing undesired thermal fluctuations.[21] Moreover, the understanding of the electronic/magnetic properties of the molecule when interacting with magnetic interfaces is of utmost importance for the development of molecular electronic field. In the following sections we will show how the electronic and magnetic properties of TbPc$_2$ are modified upon absorption on a variety of ferro- and antiferromagnetic substrates.

Coupling to Ferromagnetic Substrates

It has been shown that the stabilisation against spin fluctuation of paramagnetic molecules can be achieved through deposition of phthalocyanine/porphyrin-based molecules onto ferromagnetic substrates, taking advantage of

the planar arrangement of these molecules onto surface and the inherent close proximity between the metal ions and the ferromagnetic substrate.[21] The interaction in such systems has been found to be through superexchange and direct exchange mechanism.[21] Besides reducing the spin fluctuation and the study of the underlying physical properties of the hybrid system, deposition of molecular species onto ferromagnetic thin films also opens the possibility of heterostuctures that could be employed at higher temperatures. Interestingly, recently it was shown that molecule-substrate interactions are highly mutual, i.e. the deposition of the Mn-phthalocyanine molecules also changes considerably the magnetic properties of the underlying ferromagnetic substrate through an exchange bias mechanism.[22]

The unpaired electron delocalised on the Pc ligands ($S = \frac{1}{2}$) in the TbPc$_2$ plays an important role in the *on/off* states achieved upon STM manipulation of the Pc ligands realised by Komeda et al. on Au(111).[19] However, absorption of TbPc$_2$ on ferromagnetic substrates, might lead to total suppression of the spin character of the radical, due to the non-innocent surface-SMM interactions. Schwöbel et al. suggested the possible observation of the spin of the Pc through spin-polarised STM (SP-STM), given that the single occupied molecular orbital (SOMO) of the TbPc$_2$ unit is also the lowest unoccupied molecular orbital (LUMO), allowing its observation below and above the Fermi level, having opposite spin character.[23] Individual well separated TbPc$_2$ molecules were deposited under UHV conditions, onto cobalt islands on Ir(111). Molecule-substrate interactions seemingly similar in Cu(100) and the ferromagnetic Co substrate, where the formation of aggregates is not prompted.[13,14] Point spectroscopy allowed the investigation of the spin-averaged structure of the TbPc$_2$, resulting in two main peaks in the spin-averaged differential tunnelling conductance (dI/dU)/(I/U) at $U = -0.9$ V and $+1.3$ V, attributed to the HOMO and LUMO respectively. The topographs showed the common eight-lobes structure characteristic of π-orbital of the upper phthalocyanines groups (Fig. 5).

Figure 5. Schematic diagram of SP-STM experiments on TbPc$_2$ on Co/Ir(111) islands. (top) To obtain spin sensitivity, the magnetisation direction of the tip is aligned either parallel (green) or antiparallel (red) by applying an external

magnetic field of $B = \pm 1$ T. The Co island nanostructure (red layer) is a hard magnet with a magnetisation that does not rotate with the field applied. Because of the tunnel magnetoresistance effect, the tunnelling current depends on the relative alignment of tip and sample magnetisation directions. Examples of a spin-resolved measurement: SP-STM topographs (grey, parallel and antiparallel). Differences of maps of spin-resolved differential tunnelling conductance for right (green) $U = + 1.0$ V and left (red) $U = + 1.3$ V, providing maps of the spin polarization of the molecular orbitals. Both orbitals show the same spatial distribution, but have opposite spin polarization. Adapted with permission from ref. 23

Spin-resolved measurements, where the tungsten tip of the STM was coated with a ferromagnetic material, increasing the spin sensitivity, showed that two distinct spin channels can be probed within the $TbPc_2$. The two channels were addressed via parallel and antiparallel alignment of the STM tip and the ferromagnetic cobalt substrate, upon manipulation of the direction of the external magnetic field of ±1 T (Fig 5a).
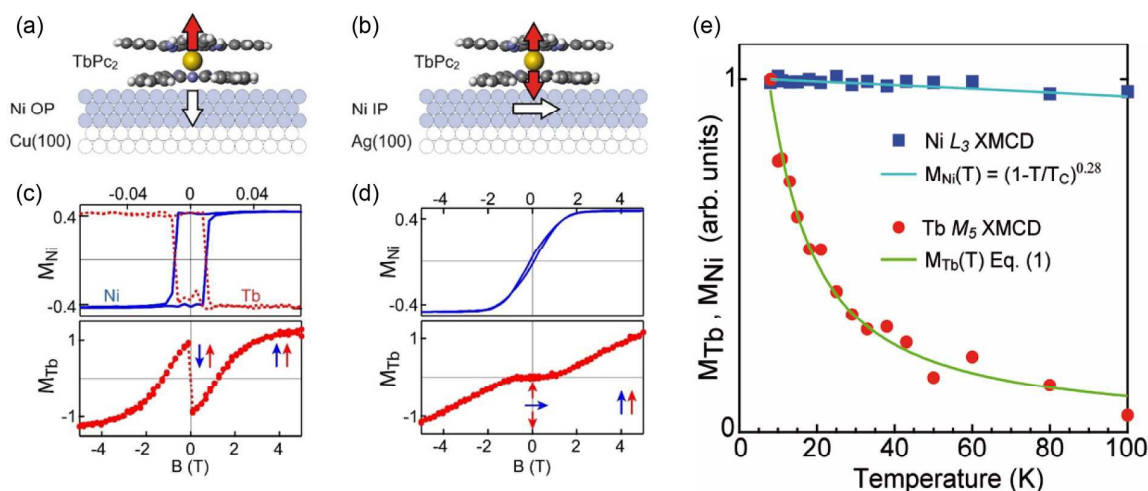
Two distinct behaviours were observed, where the difference is a measure of the spin polarization of the electron density residing on the Pcs (Fig 5a). This observation could be attributed to "spinterface" effect, in which the interaction of the lower Pc ligand with the ferromagnetic Co-substrate leads to a spin-dependent shift of the molecular energy levels, dominating the spin polarisation of the resulting tunnel current.[24] Figure 5 shows the spin polarised STM images with noticeable distinct contrast for parallel and antiparallel alignment of the STM tip and the Co island, highlighting a spin-dependence of the $TbPc_2$ molecule due to the *spinterface* effect. Constant height-mode measurements support the results, concluding that the ($S = \frac{1}{2}$) of the Pcs on Co substrate is quenched, leading to a $[TbPc_2]^-$-like configuration of the complex on the substrate.

Besides the electronic character of the $TbPc_2$ deposited on Co substrate, insight into its the magnetic properties was pursued through XMCD measurements. The studies were carried out in a $TbPc_2$ sample deposited on a 10 ML thick Co film, at $T \approx 10$ K with an external field of ±6 T, investigating the magnetisation at the Co edge (L_3) and the Tb edge (M_5).[25] Unfortunately, Klar et al. show that the data was dominated by a strong paramagnetic signal. Despite the latter issue, close to zero field an antiferromagnetic interaction of the $TbPc_2$/Co

interface was visible. No hysteresis loop was likewise observed on these measurements. Interestingly, XMCD study of $TbPc_2$ on Co surface conducted by Malavolti et al. down to 2 K and magnetic field of 3.5 T shows no sizeable magnetic coupling between the $TbPc_2$ and the Co substrate.[26] This divergence of results may be attributed to differences in the surface preparation (e.g. the importance of substrate oxidation, *vide infra*) or molecular deposition[27] and needs further understanding through additional experiments.

Rizzini and co-workers further explored the magnetic coupling between the $TbPc_2$ deposited onto a ferromagnetic nickel substrate, making use of XMCD studies.[28] The easy axis direction of the nickel substrate and the possibility of its controlled directionality through epitaxial strain made nickel an ideal candidate for the investigation. Deposition of the $TbPc_2$ was achieved *in situ* at ultrahigh vacuum conditions using molecular beam evaporation, producing a coverage of 0.05±0.02 ML of $TbPc_2$. To study the magnetic properties of the $TbPc_2$/Ni interface two magnetically different Ni films were conveyed: (*i*) an out-of-plane magnetic anisotropy Ni film (OP) and (*ii*) an in-plane magnetic anisotropy Ni film (IP). The OP Ni film was prepared by depositing Ni onto Cu(100), whereas the IP Ni film was obtained by deposition of Ni on Ag(100) (Fig. 6a,b).

Firstly, Rizzini and co-workers investigated the interaction between the $TbPc_2$ SMM and the OP Ni film, where the easy axes of both, substrate and sample are parallel, by probing the Ni ($L_{2,3}$) and Tb ($M_{4,5}$) edges using XAS and XMCD technique at 8 K. A strong remanent magnetisation was obtained for both substrate and sample. Interestingly, the XMCD of the Tb/Ni/Cu(100) (OP), revealed that the magnetic moments of the Terbium (M_{Tb}) and the Nickel substrate (M_{Ni}) were weakly antiferromagnetically coupled. Characterization of the $TbPc_2$/Ag(100) (IP) with the field applied with $\theta = 70°$ to the X-ray direction revealed a much smaller remanence of the XMCD intensity, however still highlighting the presence of antiferromagnetic interactions. Comparison of the XMCD

Figure 6. Schematic view of the $TbPc_2$ and Ni magnetisation (a) anisotropy axes of $TbPc_2$ deposited on Ni OP and (b) anisotropy axes of $TbPc_2$ deposited on Ni IP. The IP case shows spin frustration. (c) Element-resolved hysteresis loops Ni-surface-confined $TbPc_2$ exhibiting weak antiferromagnetic coupling of the collinear molecular spin in the OP case Out-of-plane (OP) Ni/Cu(100) and (d) in-plane (IP) Ni/Ag(100) films recorded at remanence, $T = 8$ K $\theta = 0°$. (e) Temperature dependence of the remanent Ni and Tb XMCD intensity, normalised to the values at $T = 8$ K, with remaining Tb-remanence at 100 K. Adapted with permission from ref. 28

results of the TbPc$_2$ onto OP and IP nickel films evidenced that stabilisation of the magnetic moment can be achieved through correct matching of the easy axis of the magnetisation between the SMM and the substrate.

In order to probe the effect of the magnetic coupling into the hysteretic behaviour of the TbPc$_2$ systems, XMCD hysteresis loops were collected for TbPc$_2$/Ni/Cu(100) (OP) and TbPc$_2$/Ni/Ag(100) (IP) substrates at T = 8 K. The data was collected at the Ni ($L_{2,3}$) and Tb ($M_{4,5}$) edges, as a function of applied magnetic field. The results are depicted in Fig. 6c and d, where atypical square-like hysteresis loops were obtained. The distinctive butterfly-like hysteretic loop commonly observed in bulk measurements of the TbPc$_2$ was clearly suppressed.[2c] The shape of the hysteresis was ascribed to antiparallel alignment of the **M$_{Tb}$** and **M$_{Ni}$**, which were very similar to the **M$_{Ni}$** square loops for B < 0.1 T. Fields larger than 0.1 T rotate the **M$_{Tb}$** leading to parallel alignment of **M$_{Tb}$** with **B**, due to continuing increase of the Zeeman energy until becoming stronger than the antiferromagnetic interaction. In an independent control experiment, the presence of remanent magnetisation (up to a temperature of 8 K) could be confirmed; equally attributed to the weak antiferromagnetic coupling to the Ni substrate.[25]

It was found that the exchange coupling was indeed mediated by the Pc group in contact with the substrate, likely occurring through electron conduction through the π-orbital of the Pc. Posteriorly, Rizzini and co-workers demonstrated that the strength of the interactions can indeed be modified through surface modification, leading to different charge transfer properties. This was achieved by addition of an electron withdrawing oxygen buffer or an electron donor such as lithium into the surface, thus leading to oxidation or reduction of the Pc ligand in contact with the Ni film. The results showed a reduction of the XMCD/XAS ratio for the TbPc$_2$/Li/Ni/Cu(100) interface, in good agreement with modest charge transfer to the 4f orbitals, due to the increased occupancy in the Pc orbitals. The magnetic behaviour was also well affected, with a noticeably decrease in the remanent **M$_{Tb}$** of the TbPc$_2$/O/Ni/Cu(100) layer and a variation of the exchange field B_{exc} from 0.6 T in the TbPc$_2$/O/Ni/Cu(100) structure to 2.5 T in the TbPc$_2$/Li/Ni/Cu(100) layer, clearly denoting that the exchange interaction is greatly increased by electron doping to the Pc orbitals. On the contrary, the oxide layer decreases the exchange molecule-metallic surface interaction; a fact showing the importance of clean deposition while working with sensitive metal surfaces.
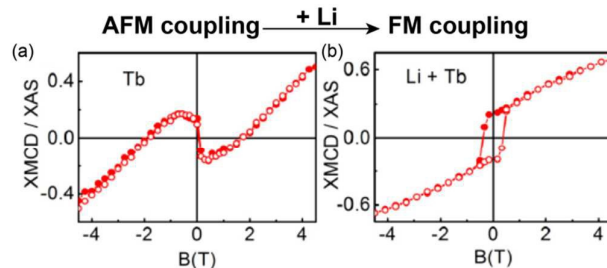
Finally, the temperature dependent behaviour of the XMCD was studied leading to observation of finite remanence of the **M$_{Tb}$** as high as 100 K (Fig. 6e), the results undoubtedly demonstrated that the interaction of the TbPc$_2$ with the nickel substrate significantly enhanced the magnetic properties of TbPc$_2$ at zero field, where 100% remanence is eluded. A result that certainly deserves to be further investigated in view of the desired higher working temperatures of spintronic devices.

The authors also compared the results for TbPc$_2$ on the ferromagnetic material and mononuclear porphyrin and phthalocyanine paramagnets on ferromagnetic substrates revealing that in mononuclear cases the exchange is ferromagnetic in nature due to the close proximity of the porphyrin/phthalocyanine metal ion and the ferromagnetic substrates, whilst in the TbPc$_2$ a larger separation favours the antiferromagnetic coupling.

Nistor and co-workers later investigated the magnetic properties of a TbPc$_2$/Fe heterostructure by depositing TbPc$_2$ onto a 4.6 ML Fe film placed on Cu(100).[29] In similar fashion to the TbPc$_2$/Ni systems, an antiferromagnetic alignment between the **M$_{Tb}$** and **M$_{Fe}$** systems was observed in XMCD loops collected at T = 8 K (Fig. 7a). At B = 1.8 T it was observed that the **M$_{Tb}$** moments changed signs overcoming the antiferromagnetic TbPc$_2$/Fe interaction leading to alignment of the **M$_{Tb}$** with the magnetic field.

The charge transfer effect was also probed by addition of Li onto the TbPc$_2$/Fe/Cu(100) heterostructure. Remarkably, the Tb magnetisation changed sign and aligns parallel to the Fe magnetisation in the whole field range, showing similar profile than that of the Fe substrate, in agreement with ferromagnetic exchange interactions (Fig. 7b).

Figure 7. XMCD Tb magnetisation curves for TbPc$_2$/Fe/Cu(100) (a) before and (b) after deposition of Li. The data were taken at T = 8 K at oblique incidence [θ = 73° for (a); θ = 60° for (b)], following field cooling in the zero field. Adapted with permission from ref. 29
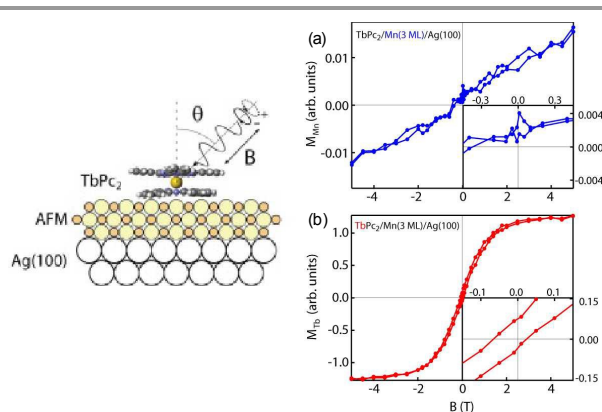
Coupling to Antiferromagnetic Substrates

The studies previously described highlights that deposition of TbPc$_2$ on ferromagnetic substrates leads to a strong enhancement of its magnetic properties, leading to finite remanence of the **M$_{Tb}$** even at 100 K, undoubtedly, representing a great advantage for certain applications were large coercivity fields are required. However, some problems are foreseen: if the magnetisation of the substrates were order of magnitude higher than the molecular species and the magnetic moment is tightly connected to the substrate magnetisation, it would become impossible the independent manipulation of the magnetic moment of the molecule from the substrate. A different alternative for the stabilisation and enhancement of the magnetic behaviour is through deposition of the SMM onto antiferromagnetic substrates. Several issues with this proposal have been discussed by Rizzini et al.,[6d,30] however the investigation of the TbPc$_2$ AFM substrate led to some degree of understanding of the magnetic properties of the heterostructures. In the following sections we will briefly discuss the magnetic properties of TbPc$_2$ deposited on antiferromagnetic substrates such as CoO, Mn and FeMn.

On the quest of exchange bias effects on TbPc$_2$ deposited on antiferromagnetic (AFM) substrates, Rizzini and co-workers

studied a TbPc$_2$ deposited on a 10 ML thick CoO layer, chosen as substrate due to its magnetocrystallinity, and the facile tuning of magnetic anisotropy.[30] The surface was prepared *via* molecular beam epitaxy in ultrahigh vacuum, followed by *in situ* deposition of TbPc$_2$ at UHV conditions. The sample was posteriorly cooled down to 8 K in an applied field of 5 T, normal to the surface. XAS measurements were then conducted on the Co and Tb edges respectively, with a magnetic field of ± 5 T applied parallel to the X-ray incidence radiation. As expected, due to the AFM nature of the substrate, and very few uncompensated polarised Co spins, a very weak XMCD response was recorded. Conversely, the TbPc$_2$ XMCD data showed a strong XMCD response, after saturation at +5 T. No hysteresis was found in the XMCD loop of the Tb^{3+} ion, showing no sizeable exchange bias of the heterostructure. It was likewise observed some inflections at B = ± 0.5 T, consistent with the butterfly-like hysteresis observed on bulk. Notably, they vanish upon charge doping. In light of the result, the authors proceeded to study the thickness dependence of the CoO film, resulting in not clear indication of exchange bias. These results suggest that the CoO AFM substrate is not suitable for exchange bias molecule-substrate structures, in good agreement with the behaviour observed for the TbPc$_2$/O/Ni/Cu(100) heteroestructure, where a weaker exchange interaction was found.

The previous results showed that oxygen covered substrates prompted weak molecule-substrate interactions compared to neat metallic surfaces (*vide supra*). To test whether the same reasoning held for oxygen free AFM structure, the XMCD properties of TbPc$_2$ deposited on bare Mn were investigated. The sample studied comprised 3 ML of Mn film deposited on Ag(100). The XMCD of the Mn edge showed an extremely weak signal (compared to the paramagnetic Mn sample), highlighting the AFM nature of the Mn substrate. A field dependent behaviour of the XMCD intensity was additionally observed, implying uncompensated Mn spins, some of them able to rotate whilst others remaining pinned to the structure (~7 %), whilst the total of uncompensated spins was ca. 3 %.

Finite hystereses were detected through XMCD experiments of the TbPc$_2$/Mn/Ag(100) sample, with a coercivity of H_C = 44.±4 mT, whilst shifting of H_E = −22±4 mT was observed for M_{Tb}, signatures of exchange bias. The observations e.g. sign and shift, are in good agreement with the low field XMCD data shown in Fig. 8.

Figure 8. Exchange bias between TbPc$_2$ and Mn. Magnetisation loops of Mn (a) and Tb (b) measured on TbPc$_2$/Mn(3 ML)/Ag(100), after FC at θ = 0° and B = 5 T, recorded at θ = 0° and T = 8 K. Inset: Detail of the low field region. Units refer to the intensity ratio 2($I^+ − I^-$)/(I+ + I−) measured at the L_3 Mn edge (a) and M_5 Tb edge (b). ref. 30

The authors hypothesised that due to the skewed shaped loop and the small remanence of the M_{Tb}, only a small fraction of the on-surface TbPc$_2$ were exchange-coupled to the unpinned spins of the Mn substrate. This is consistent with the small fraction of unpinned spins of the Mn substrate and in contrast with the TbPc$_2$/Ni/Cu(100) case, where the squared-shaped hysteresis loops indicate that most TbPc$_2$ molecules were interacting with the Ni substrate. Due to the average detection mode of XMCD over all molecules interacting and not interacting, it could in principle be possible to obtain H_E and H_C much larger if the measurements could be conducted solely on interacting TbPc$_2$.

A comparative study of TbPc$_2$ on ferromagnetic and antiferromagnetic substrates was conducted by Gambardella's group.[29] The study was performed employing ferromagnetic Fe and antiferromagnetic FeMn substrates. While the description of the former has been previously addressed (*vide supra*), we focus our attention in this section to the antiferromagnetic FeMn substrate and its interaction with the TbPc$_2$.

Three TbPc$_2$/FeMn/Cu(100) samples with different FeMn thicknesses (3, 6 and 8 ML) were prepared by electron beam evaporation of Fe and Mn on Cu(100) substrate at room temperature, whilst TbPc$_2$ was sublimed on the surface using a molecular beam epitaxy cell with a flux rate of 0.8 ML/min. The final TbPc$_2$ coverage was 0.6±0.1 ML. XAS and XMCD measurements indicated that in the surface most of the FeMn spins were compensated, with parallel alignment of the M_{Fe} and M_{Mn} with the external magnetic field. The magnetic moment on the Tb^{3+} ions was almost saturated at the experimental temperature and field. All samples showed some hysteretic behaviour, with the more pronounced hysteresis observed in the sample with thickest FeMn coverage i.e. TbPc$_2$/FeMn(8 ML)/Cu(100), which along with the shift in field, indicated that the antiferromagnetic regime was reached.

A coercivity H_C = −10±1 mT and a field displacement of H_E = 21±1 mT was obtained from magnetisation curves of Tb, the effect arising from exchange interactions with the pinned Fe ions on the surface. The results showed that the TbPc$_2$/FeMn/Cu(100) exhibit antiferromagnetic interactions. Relatively strong TbPc$_2$/FeMn substrate interaction can be

inferred form the absence of the butterfly-like hysteresis loop and the plateaus in the Tb magnetisation curve.

Grafting TbPc$_2$ to Non-Metallic Substrates

As shown up to this point, the electronic and magnetic properties of the TbPc$_2$ SMM are highly affected by the substrate where deposited due to hybridization with the Pc orbitals, leading to improved magnetic behaviours, as observed in the TbPc$_2$ on Ni films, or preclusion the hysteretic magnetic properties of the TbPc$_2$ as observed on CoO. In order to observe the inherent magnetic properties of the TbPc$_2$ at molecular level, less interacting substrates are envisaged. In this context, grafting of TbPc$_2$ on highly conjugated carbon containing materials such carbon nanotubes (CNT), graphene, highly oriented pyrolytic graphite (HOPG) or insulators such as SiO$_2$ and MgO seems promising. Deposition of TbPc$_2$ on these substrates would limit the number of electrons migrating between the molecule and surface, therefore allowing the observation of less perturbed magnetic properties of the SMM. Furthermore, several manipulation schemes can be envisaged for a molecule on a sp^2-carbon substrate, expanding the research interest.   Similarly, the exploration of the magnetic properties of TbPc$_2$ on insulators can shed some light into the type of tunnelling events occurring when the TbPc$_2$ is in contact with strongly interacting substrates.

Grafting TbPc$_2$ to sp^2-carbon-containing substrates

In this section the magnetic and electronic properties of TbPc$_2$ on single-walled carbon nanotubes (SWCNT), graphene and highly oriented pyrolytic graphite (HOPG) will be surveyed. The authors have shown that due to the weak TbPc$_2$-substrate interactions, a more bulk-like magnetic behaviour is detected, leading to several spintronic proposals for the physical implementation of TbPc$_2$ in technological applications.
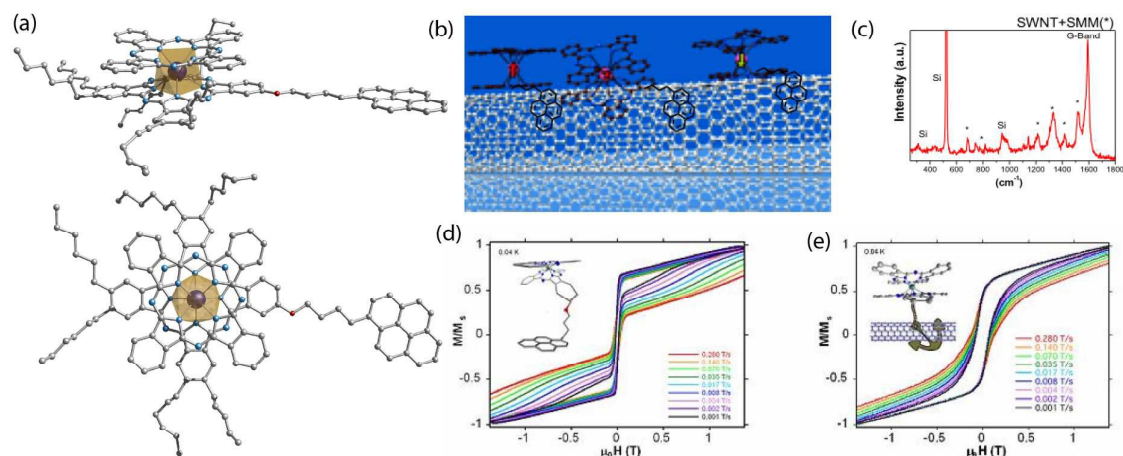
In 2009 Klyatskaya and co-workers firstly explored the magnetic properties of a chemically modified version of the well-known TbPc$_2$ when attached to single-walled carbon nanotubes (SWCNT) through a range of physical and magnetic techniques.[31] SWCNT were chosen as substrates due to their relevance in technological applications and cross-section, analogous to that of the TbPc$_2$. In the study, a tailored designed version of the TbPc$_2$ was chemically engineered and synthesised. The molecule comprised an heteroleptic TbPc$_2$ molecule, where one of the phthalocyanine ligands is substituted with three hexyl groups and one 4-(4-Pyren-1-ylbutoxy) group (from now on called TbPc$_2$*). It has been observed that the hexyl and the pyrene groups show considerable π-π stacking to sp^2-carbon containing materials. The TbPc$_2$* was attached to SWCNT and characterised through a range of surface techniques, revealing that TbPc$_2$* molecule were grafted to the CNT (Fig. 9).

In order to probe whether the magnetic properties of the SWCNT-SMM hybrid were present, AC susceptibility measurements were conducted showing a clear maximum in the $\chi''(T)$ at 45 K (1 kHz) yielding a U_{eff} = 500 K. Interestingly, the dynamic magnetic behaviour showed an enhancement of the dynamic properties, compared to the diluted TbPc$_2$ sample. Confirmation of the magnetic properties of the TbPc$_2$* was gained through μ-SQUID measurements at 40 mK. As observed in Fig. 9d,e, hysteresis loops were observed at different scan rates, confirming that the magnetic properties of the TbPc$_2$* in the SWCNT-SMM were present. Step-like loops were not detected due to smearing effect of the randomly oriented TbPc$_2$* on the SWCNTs.

The chemically engineered TbPc$_2$*-SWCNT hybrid has been subject of a number of state-of-the-art investigations as a molecular spin valve device, leading to the observation of magneto resistivity, strong spin-phonon coupling, Landau-Zener tunnelling, and suppression of quantum tunnelling of magnetisation (QTM).[32]
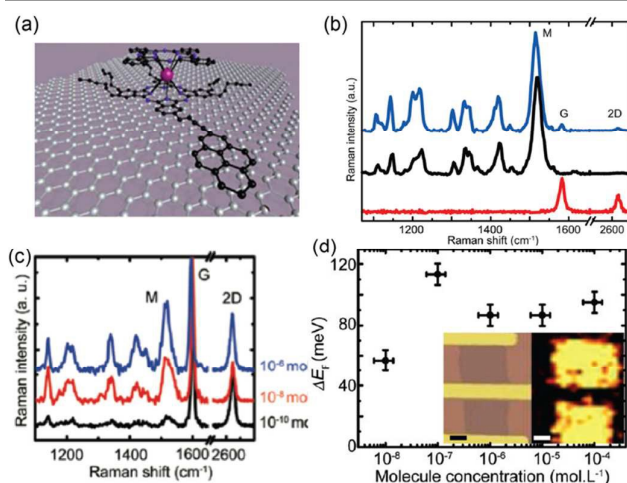
The intriguingly impressive electrical and mechanical properties of graphene make it a promising material in spintronic[33], electronic[34] and nanomechanic applications.[35] In

Figure 9. The TbPc$_2$*-confinement on SWCNTs (a) Crystal structure of the pyrene-substituted TbPc$_2$* side and top view. Lower panel shows the polyhedral representation of the TbN$_8$ coordination environment with D_{4d}-square-antiprismatic coordination geometry. Colour code: C, grey; N, cyan; Tb, dark blue. Hydrogens were omitted for clarity. (b) schematic representation of the surface confinement; (d) μ-Raman spectra of the SWCNT-SMM hybrid showing the fingerprint of both TbPc$_2$*-and the SWCNT. (d) μ-SQUID measurements of (left) the TbPc$_2$* bulk and (right) the SWCNT-SMM hybrid exhibiting reduced QT rates at zero field sue to reduced dipole-dipole interactions. Adapted with permission from ref. 31

the light of the behaviour observed for TbPc$_2$* grafted on CNT and the bewildering properties of graphene it was immediately prompted the investigation of the coupled behaviour of the SMM and graphene. For the study, molecular grafting of the TbPc$_2$* through π-π stacking was envisioned, which beside the grafting properties of the pyrene and hexyl groups, the anchoring groups additionally mediated indirect coupling as observed on CNT.[32] Atomic force microscopy (AFM) and Raman studies showed that upon grafting the TbPc$_2$* unit was intact as well as the graphene substrate (Fig. 10). AFM roughness analysis indicates the formation of molecular clusters formed by less than five molecules at concentration lower than 10^{-5} mol L^{-1} whereas higher concentrations lead to the formation of much larger clusters aggregates. A slight shift of the G band of graphene was also observed in Raman spectrum, consistent with small interaction of the TbPc$_2$* to the surface.[36]

To obtain more insight regarding the thickness of TbPc$_2$* on graphene and its effect, AFM contact mode and Raman maps experiments were conducted, showing a logarithmic dependence of the Raman intensity of the deposited TbPc$_2$*, in good agreement with the enhancement through molecular variation of the polarizability via charge transfer of the substrate, occurring only in the limit of molecules directly interacting with the graphene substrate, i.e. thicker films would not dramatically enhance the Raman intensity. The authors estimated the enhancement of the SMM signal grafted on graphene to be as low as 10^{-10} mol L^{-1}. Ab initio density functional theory calculations were likewise computed, employing just the pyrene fragment of the TbPc$_2$*, for computational reasons. The results show that the G band of the graphene shifts slightly to lower frequencies, in excellent agreement with doping-induced change of the Fermi level, indicating that the behaviour comes just from the molecules directly interacting with the graphene substrate (Fig. 10 a,b). A molecular spin valve like device was also constructed based on a contacted graphene-TbPc$_2$* hybrid.[37]

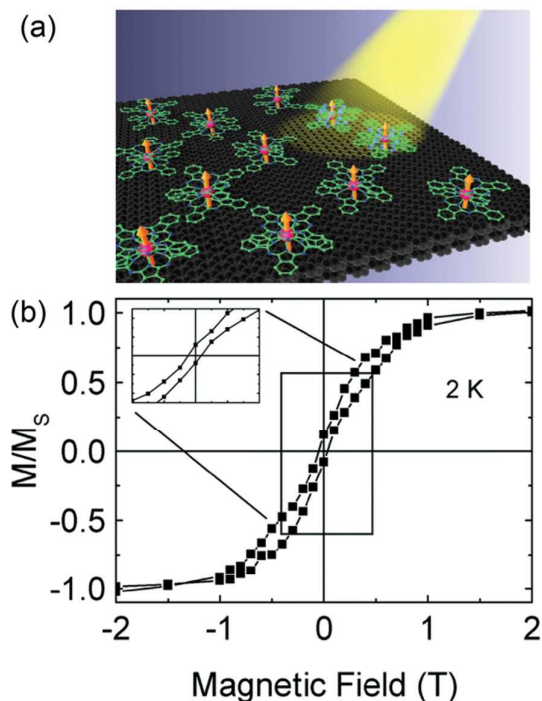**Figure 10.** (a) Scheme of TbPc$_2$* grafted to graphene. (b) Raman spectra of the neat graphene (bottom, red), TbPc$_2$ powder (middle, black), and TbPc$_2$ molecules onto graphene (top, blue). The G and 2D modes of graphene and the M band of TbPc$_2$ molecules are indicated. (c) Raman spectra of TbPc$_2$ molecules deposited on graphene at three concentrations. (d) Concentration dependence of the shift of the Fermi energy relative to the pristine device. Inset: optical image and

Raman intensity map of the M doublet of the device (scale bars 1 m). Adapted with permission from ref. 36

Moreover, the self-assembly and magnetic behaviour of an analogue of TbPc$_2$ on highly ordered pyrolytic graphite (HOPG) was first performed by Veciana et al. in 2006[38], and later continued by Godinec et al in 2011.[39] The subject of investigation was a double decker terbium phthalocyanine complex with formula Tb^{i}Pc$_2$ where ^{i}Pc = tetrakis-isopropylidenedioxy-phthalocyanine, deposited on the HOPG substrate through drop casting technique with a 10^{-6} M solution. AFM experiments showed highly regular bar-like islands motifs of Tb^{i}Pc$_2$ on the surface, with regular orientation of ca. 120° between the bars, suggesting that the growth of these supramolecular islands occur along one of the three principal graphite symmetry directions.

In order to probe whether any interaction of the Tb^{i}Pc$_2$-HOPG sample could diminish the SMM behaviour, the authors systematically studied the magnetic properties of two different Tb^{i}Pc$_2$-HOPG through XMCD spectroscopy: (i) a submonolayer and (ii) thick layer sample, after drop casting Tb^{i}Pc$_2$ in HOPG. The authors expected a more pronounced and surface dependent XMCD behaviour of the thin layer sample and a more bulk-like behaviour for the multi-layered sample. The hysteresis loops for both samples were obtained at θ = 0 and 45° grazing angles in relation to the applied magnetic field measured at the $M_{4,5}$ Tb edge after magnetizing the samples up to 5 T followed by demagnetisation. The results showed butterfly-like hysteretic loops, with a small remnant magnetisation for both samples, demonstrating that in both cases the magnetic behaviour was very similar and that Tb^{i}Pc$_2$-HOPG interaction had little effect on the surface deposited SMM.

More recently Klar and co-workers reported the hysteretic behaviour of TbPc$_2$ on HOPG at very low temperatures.[40] Deposition of TbPc$_2$ was achieved by *in situ* thermal evaporation of pristine TbPc$_2$ on freshly sliced HOPG crystal under UHV conditions. The XAS spectra of Tb was measured at several angle i.e. θ = 0, 45 and 65° X-ray angles at *T* = 2 K and external magnetic field of 6 T, which affords no XMCD shape change in relation to the angle variation, with only changes in the magnitude of the XMCD signal (Fig. 11).

Figure 11. (a) Schematic representation of TbPc$_2$ grafted to HOPG. (b) XMCD loop of TbPc$_2$ on HOPG taken at the Tb M_5 edge at T = 2 K. Adapted with permission from ref. 40

The field dependent study at 2 K showed that the saturation of the magnetisation was achieved at 1 T, with a well-defined opening of the hysteresis loops with coercive field of ca. 50 mT. Remarkably, just small narrowing close to B = 0 was present in the hysteresis, with no closing of the loop at zero field, usually associated to fast QTM often affording butterfly-like hysteresis. This effect was ascribed to slower quantum tunnelling at this temperature and reduced interaction of TbPc$_2$ with the surroundings when deposited on HOPG.
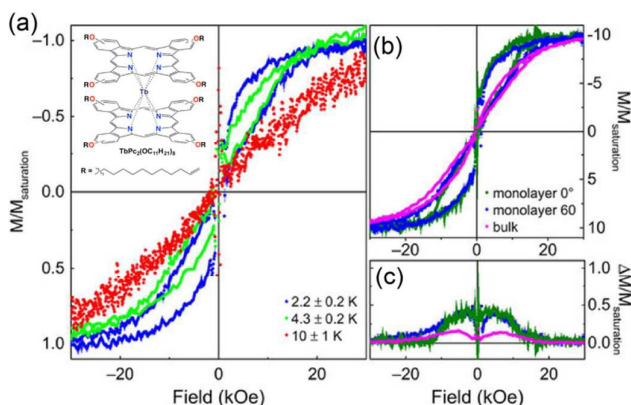
TbPc$_2$ on Insulators

In the previous section it was shown that upon deposition of TbPc$_2$ on sp^2-based substrates the magnetic properties of the SMM are less perturbed due to the weak coupling between the substrate and the SMM, leading to the observation of hysteresis with less QTM near zero field. In the HOPG and SWCNT cases more precisely, through XMCD and conductivity experiments it was found that reduction of the quantum tunnelling can be achieved, affording less QTM close to zero applied field. On the quest of wider hysteresis loops at higher temperatures, recently some researchers have turned their attention towards insulators materials such SiO$_2$ and MgO, where the substrate can act as a tunnelling barrier. Moreover, the study of TbPc$_2$ on insulators such as SiO$_2$, a high quality electrical insulator and MgO acting as barrier in spin-tunnelling barriers, is of utmost relevance given their technological relevance an applicability in device production. In this section the magnetic properties of TbPc$_2$ on these two insulator substrates will be surveyed.

Silicon besides being a well-known electrical insulator also offers the possibility of doping, which could be employed as a tool for the manipulation of the electronic properties of the deposited sample. As observed, the on-surface Pc group is very susceptible to electronic properties of the substrates, which in turn is reflected on the magnetic properties of the Tb^{3+} ion due to the coupling between the unpaired π-electron delocalised over the Pc groups and the J = 6 of the Tb ion, making SiO$_2$ a very promising substrate for hybrid devices. With this aim in mind and the quest of understanding of the magnetic properties of TbPc$_2$ on SiO$_2$ substrate Mannini et al. studied of the magnetic properties of an analogue of TbPc$_2$ complex through XMCD measurements.[41] The approach consisted in the chemical deposition and grafting of a functionalised TbPc$_2$, namely TbPc$_2$(OC$_{11}$H$_{21}$)$_8$, which allowed direct Si-C bounds via thermal hydrosilylation. Structural characterization of the compound was achieved via a MALDI-Tof, UV-Visible, X-ray photoelectron spectroscopy (XPS) and NMR techniques, whilst the bulk magnetic properties were probed through AC magnetometry, all together validating the proposed structure and the SMM character of the sample.

Following characterization of the bulk sample, a monolayer of TbPc$_2$(OC$_{11}$H$_{21}$)$_8$ was grafted to a SiO$_2$(100) wafer through hydrosilylation, leading to direct linking between of TbPc$_2$(OC$_{11}$H$_{21}$)$_8$ to the SiO$_2$ surface via Si-C bonds. The substrate was afterwards subjected to several cleaning procedures to ensure that just the chemically bound TbPc$_2$(OC$_{11}$H$_{21}$)$_8$ were present on the surface. XPS analysis of the TbPc$_2$(OC$_{11}$H$_{21}$)$_8$/SiO$_2$(100) system confirmed that the molecules were grafted to the surface. Interestingly, XPS spectra also revealed two peaks in the spectrum of the monolayer film compared to a single peak observed in thicker film prepared by drop casting procedure. The authors ascribed the appearance of the second peak to a possible oxidised form of the TbPc$_2$(OC$_{11}$H$_{21}$)$_8$, which could be surface-induced effect. The XPS results were further supported by DFT calculations.
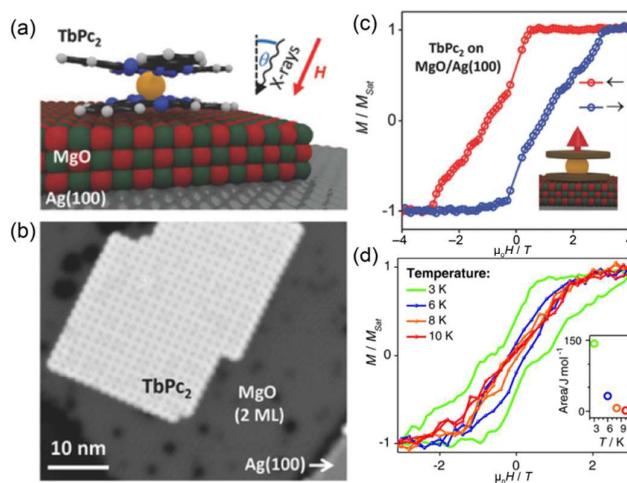
XNLD measurements performed on the TbPc$_2$(OC$_{11}$H$_{21}$)$_8$/SiO$_2$(100) sample at the $M_{4,5}$ Tb edges posteriorly showed that most molecules lay with face-on configuration on the SiO$_2$(100) surface, as commonly observed for TbPc$_2$. On the other hand, XMCD measurements at low temperature with a magnetic field of 5 T parallel to the X-ray light propagation vector measured at the M_5 edge of Tb affords hysteresis loops down to 4.3 K. The authors compared the loops of the monolayer sample with that of a drop casted thick film on SiO$_2$ (with bulk-like magnetic properties) revealing smaller opening of the loop in the latter case (Fig. 12). As observed in Fig. 12b the monolayer showed a larger hysteresis compared to that of the bulk-like material. The authors moreover proposed that upon chemical binding of the TbPc$_2$(OC$_{11}$H$_{21}$)$_8$ to the SiO$_2$ substrate an oxidizing-like effect could take place therefore enhancing the magnetic properties of the TbPc$_2$(OC$_{11}$H$_{21}$)$_8$, as shown for TbPc$_2$$^+$.[10b] Unfortunately, albeit depositing TbPc$_2$ on an insulator substrate, the quantum tunnelling at zero field was still present.

Figure 12. (a) XMCD hysteresis curves for θ = 60° as a function of the temperature in the TbPc$_2$(OC$_{11}$H$_{21}$)$_8$@Si monolayer. (b,c) Comparison between the behaviour of the thick film and the monolayer, the latter being measured for θ= 0° and 60°. These magnetisation curves, measured in the same condition for all the samples (2.2±0.2 K and 500 Oe s^{-1} scan speed) through the XMCD technique, are reported in b with their experimental error. In c, the hysteresis opening is estimated as Δ*M*(*H*) according to the procedure described in the text. Adapted with permission from ref. 41

Although hysteretic magnetic behaviour was afforded upon deposition of an analogous TbPc$_2$ on SiO$_2$ after chemical grafting, the collected hystereses were narrow and with visible QTM at zero field, indicating that efficient suppression of QTM is not achieved. Recently, through a similar approach the record hysteresis for a surface deposited SMM was realised after depositing TbPc$_2$ on a MgO insulating layer deposited onto Ag(100) with composition TbPc$_2$(0.6 ML)/MgO(5 ML)/Ag(100).[42] STM analysis confirmed that the TbPc$_2$ molecules maintain flat arrangement on the surface leading to 2D islands on the MgO surface, showing the typical eight-lobed pattern from the staggered configuration of the Pc groups. XNLD also corroborated the face-on configuration of the TbPc$_2$ on the MgO film supporting the STM observations (Fig. 13a).

XMCD measurements showed a strong remanence of the magnetisation with hysteresis loops opening up to 3 T at 3 K, demonstrating that the QTM has been strongly suppressed (Fig. 13c). In order to obtain some insight into the mechanism leading to suppression of the QTM on the TbPc$_2$/MgO/Ag(100), the authors studied three other samples: (*i*) a multi-layered TbPc$_2$ deposited on MgO film; (*ii*) TbPc$_2$/Ag(100) and (*iii*) TbPc$_2$ deposited on a well-known insulator such hexagonal boron nitride (*h*-BN). The results unveiled strong quantum tunnelling when TbPc$_2$ is deposited on bare Ag(100) with nearly closing of the hysteresis loop at 3 K, whilst when multi-layered TbPc$_2$ was deposited on a MgO film, the QT is reduced compared to the TbPc$_2$/Ag(100) but increased when compared to the monolayer TbPc$_2$/MgO/Ag(100) sample, attributed to magnetic interaction between neighbouring TbPc$_2$ molecules in the dense packing (See Fig. 13c,d).

Figure 13. Self-assembly and exceptional magnetic remanence and hysteresis of TbPc$_2$ molecules on insulating MgO films. (a) Sketch of a TbPc$_2$ molecule on an ultrathin MgO film on Ag(100). (b) Scanning tunnelling microscopy image revealing self-assembled arrays of TbPc$_2$ on two monolayers (MLs) of MgO. (c) Hysteresis loop obtained with XMCD at 3 K for 0.6 ML TbPc$_2$ on 5 ML MgO. (d) Temperature-dependent magnetisation curves of TbPc$_2$/MgO/ Ag(100). With increasing temperature, the magnetisation loop gradually closes until the hysteresis fully vanishes at 10 K (X-ray flux *Φ*$_0$, 0.3 ML TbPc$_2$ on 4.8 ML MgO). The area of the hysteresis opening is plotted in the inset. Adapted with permission from ref. 42

Studies of TbPc$_2$ on *h*-BN likewise showed some degree of suppression of the QT, however due to the intrinsic monolayer self-assembly properties of *h*-BN, compared to MgO, suppression of the QT is not as effective as in the MgO case. Given that TbPc$_2$ self-organization on MgO, *h*-BN and Ag(100) surfaces was similar, with face-on arrangement, the authors were able to ascribe the wide hysteresis loops to the insulating properties of MgO. Temperature dependent hysteresis loops measurements were carried out affording slow relaxation of the magnetisation above up to 8 K, the highest blocking temperature reported for a surface-deposited SMM (Fig. 13d). The magnetic remanence and wide hystereses loops of TbPc$_2$ on MgO were attributed to the suppression of the electron fluctuations and scattering on the surface by the MgO barrier, with an exponential dependence of the tunnelling rate with the MgO thickness.

Furthermore, the authors also propose that the magnetic behaviour could be attributed to a minimum TbPc$_2$-MgO hybridization, which leads to practically no distortion of the *D*$_{4d}$ symmetry of the TbPc$_2$ on the surface, therefore less QT is prompted. Moreover, comparison of the XMCD of monolayer and multilayer TbPc$_2$ on MgO showed that lateral (horizontal) exchange interactions play a smaller role in the tunnelling events, whilst vertical interactions enhance magnetic relaxations.

Conclusions

In the quest of molecular spintronic devices made from SMMs, it has become clear that the confinement of magnetic molecules in the proximity of surfaces and electrodes has similar impact onto the magnetic performance of the SMMs as

found in molecular engineering approaches, e.g. creating strongly axial ligand fields,[43] or by introducing exchange bias.[4d]

The results of several authors show that upon deposition of the $TbPc_2$ SMM on different substrates both enhancement or quenching of the hysteresis loops is achieved depending solely on the nature of the substrate. Deposition of $TbPc_2$ at monolayer coverage on non-magnetic metallic substrates yields practically unopened hysteresis loops, despite the unperturbed nature of the Ising-type behaviour of the Tb^{3+} ion. Only a very small opening of the magnetic hysteresis was observed at 2 K when $TbPc_2$ was deposited on Au(111). This fact can be ascribed to accelerated QT rates of the SMM via spin–phonon interface, but also to metal-π-orbital hybridization and changing of the dipole-dipole coupling paths, evidencing that strong interactions are harmful to the SMM properties when deposited on these surfaces.

Astonishingly, deposition of $TbPc_2$ on magnetic substrates have the contrary effect. $TbPc_2$ on ferromagnetic substrates such as nickel, leads to antiferromagnetic coupling of the molecular $J = 6$ spin to the out-of-plane magnetic moment of the nickel substrate, attributed to an exchange mechanism, present even after the insertion of a graphene layer between the $TbPc_2$ and Ni substrate.[44] Remarkably, the observation of finite remanence of the $\mathbf{M_{Tb}}$ as high as 100 K demonstrates how the SMM-ferromagnetic-substrate interactions can significantly enhance the magnetic properties of $TbPc_2$ at zero field. Likewise, on the quest of the systematic manipulation of the substrate-molecule exchange interaction it has been shown that upon addition of electron withdrawing or donor agents to the surface some degree of control can be attained. Recently, Candini et al. have also shown that a similar effect is achieved by changing the anisotropic lanthanide ion residing in the double decker SMM.[45] A much weaker, although sizeable, interaction is achieved after deposition of the SMM on antiferromagnetic substrates such Mn, leading to the observation of exchange bias mechanism. These are very promising results on the ongoing search for increased working temperatures for future molecular spintronic devices.

Conversely, $TbPc_2$ on less interacting substrates as HOPG leads to some degree of suppression of QT neat zero field, due to weak interaction of the $TbPc_2$ with the HOPG surface. The results on graphene and SWCNTs undoubtedly highlights the pivotal role of the control of the spin-phonon coupling. By suspending SWCNTs and exploiting their quantum properties (e.g. discrete phonon energies of the SWCNTs)[32d] it is possible to suppress completely the QT in a surface-confined $TbPc_2$ SMM.

Finally, more efficient suppression of the QT rate is achieved on insulators as SiO_2 and MgO, leading to the observation of a giant hysteresis up to 8 K in the latter case, emphasising the importance of insulating layers on the magnetic properties of the SMM, setting a new scenario towards SMM-based tunnel devices. In addition, these results demonstrate that engineering the spin-phonon coupling at the molecule-substrate interface is a valid approach in the long-lasting search for increased blocking temperatures of SMMs.

It is evident that for a successful implementation of SMM on quantum computing or tunnelling devices a thorough understanding of the magnetic behaviour of SMMs at the surface level is as necessary as the understanding of properties of the surface where deposited. As final remark, although this perspective article has been entirely devoted to surface-confined $TbPc_2$, the understanding of the magnetic characteristics of this SMM on surfaces offers the scientific community some flavour of the underlying characteristics of on-surface SMMs, which must be taken into consideration for the realisation of hybrid SMM-spintronic devices.
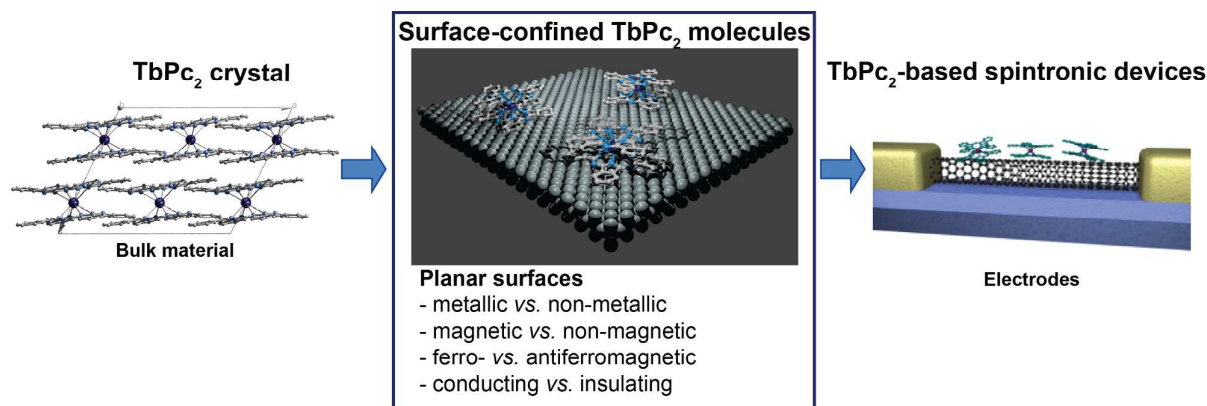
Acknowledgments

References

1   (a) D. Gatteschi, R. Sessoli, J. Villain, *Molecular Nanomagnets*; Oxford University Press: Oxford, 2006.
2   (a) N. Ishikawa, M. Sugita, T. Ishikawa, S.-Y. Koshihara and Y. Kaizu, *J. Am. Chem. Soc.* 2003, **125**, 8694; (b) N. Ishikawa, M. Sugita, T. Okubo, N. Tanaka, T. Iino and Y. Kaizu, *Inorg. Chem.* 2003, **42**, 2440; (c) N. Ishikawa, M. Sugita and W. Wernsdorfer, *Angew. Chem. Int. Ed.* 2005, **44**, 2931; (d) N. Ishikawa, M. Sugita, T. Ishikawa, S.-Y. Koshihara and Y. Kaizu, *J. Phys. Chem. B* 2004**, 108**, 11265.
3   (a) D. N. Woodruff, R. E. P. Winpenny and R. A. Layfield, *Chem. Rev.* 2013, **113**, 5110; (b) R. Sessoli and A. K. Powell, *Coordin. Chem. Rev.* 2009, **253**, 2328; (c) J. Luzon and R. Sessoli, *Dalton Trans.* 2012, **41**, 13556; (d) L. Sorace, C. Benelli and D. Gatteschi, *Chem. Soc. Rev.* 2011, **40**, 3092.
4   (a) M. Gregson, N. F. Chilton, A. M. Ariciu, F. Tuna, I. F. Crowe, W. Lewis, A. J. Blake, D. Collison, E. J. L. McInnes, R. E. P. Winpenny, and S. T. Liddle, *Chem. Sci.* 2016, **7**, 155; (b) J. Liu, Y.-C.; Chen, J.-L. Liu, V. Vieru, L. Ungur, J.-H. Jia, L. F. Chibotaru, Y. Lan, W. Wernsdorfer, S. Gao, X.-M. Chen and M.-L. Tong, *J. Am. Chem. Soc.* 2016, **138**, 5441; (c) J. D. Rinehart, M. Fang, W. J. Evans and J. R. Long, *Nat. Chem.* 2011, **3**, 538; (d) T. Pugh, N. F. Chilton, R. A. Layfield, *Angew. Chem. Int. Ed.* 2016, DOI: 10.1002/anie.201604346.
5   J. J. Dreiser, *Phys.: Condens. Matter* 2015, **27**, 183203.
6   (a) M. Mannini, F. Pineider, P. Sainctavit, C. Danieli, E. Otero, C. Sciancalepore, A. M. Talarico, M.-A. Arrio, A. Cornia, D. Gatteschi, and R. Sessoli, *Nat. Mater.* 2009, **8**, 194; (b) L. Sorace, A. Cornia and R. Sessoli, *Nature* 2010, **468**, 417; (c) G. Poneti, L. Poggini, M. Mannini, B. Cortigiani, L. Sorace, E. Otero, P. Sainctavit, A. Magnani, R. Sessoli and A. Dei, *Chem. Sci.* 2015, **6**, 2268; (d) A. L. Rizzini, C. Krull, A. Mugarza, T. Balashov, C. Nistor, R. Piquerel, S. Klyatskaya, M. Ruben, P. M. Sheverdyaeva, P. Moras, C. Carbone, C. Stamm, P. S. Miedema, P. K. Thakur, V. Sessi, M. Soares, F. Yakhou-Harris, J. C. Cezar, S. Stepanow, and P. Gambardella, *Surf. Sci.* 2014, **630**, 361; (e) C. Cervetti, A. Rettori, M. G. Pini, A. Cornia, A. Repollés, F. Luis, M. Dressel, S. Rauschenbach, K. Kern, M. Burghard, and L. Bogani, *Nat. Matter.* 2016, **15**, 164.
7   See for example: (a) M. L. Baker and H. Mutka, *Eur. Phys. J. Spec. Top.* 2012, **213**, 53; (b) E. J. L. McInnes, *Spectroscopy of Single-Molecule Magnets. In Single-Molecule Magnets and*

Related Phenomena; Structure and Bonding; Springer-Verlag: Berlin/Heidelberg, 2006; Vol. 122, pp. 69–102; (c) M. Gonidec, E. S. Davies, J. McMaster, D. B. Amabilino and J. Veciana, *J. Am. Chem. Soc.* 2010, **132**, 1756.

8   See for example: (a) W. Wernsdorfer, K. Hasselbach, A. Benoit, B. Barbara, D. Mailly, J. Tuaillon, J. P. Perez, V. Dupuis, J. P. Dupin, G. Guiraud and A. Perex, *J. Appl. Phys.* 1995, **78**, 7192; (b) G. Cucinotta, M. Perfetti, J. Luzon, M. Etienne, P.-E. Car, A. Caneschi, G. Calvez, K. Bernot and R. Sessoli, *Angew. Chem. Int. Ed.* 2012, **51**, 1606.

9   (a) R. Sessoli, D. Gatteschi, A. Caneschi, and M. A. Novak, *Nature*, 1993, **365**, 141; (b) R. Sessoli, H.-L. Tsai, A. R. Schake, S. Wang, J. B. Vincent, K. Folting, D. Gatteschi, G. Christou and D. N. Hendrickson, *J. Am. Chem. Soc.* 1993, **115**, 1804.

10 (a) C. R. Ganivet, B. Ballesteros, G. d. Torre, J. M. Clemente-Juan, E. Coronado and T. Torres, *Chem. Eur. J.* 2012, **19**, 1457; (b) S. Takamatsu, T. N. Ishikawa, *Polyhedron* 2007, 26, 1859.

11 L. Vitali, S. Fabris, A. M. Conte, S. Brink, M. Ruben, S. Baroni and K. Kern, *Nano Lett*. 2008, **8**, 3364.

12 (a) G. V. D. Laan, *J. Phys.: Conf. Ser.* 2013, **430**, 012127; (b) J. Stöhr, *J. Magn. Magn. Mater*. 1999, **200**, 470; (c) T. Funk, A. Deb, S. J. George, H. Wang and S. P. Cramer, *Coord. Chem. Rev.* 2005, **249**, 3; (d) G. van der Laan, and A. I. Figueroa, *Coord. Chem. Rev.* 2014, **277**, 95.

13 S. Stepanow, J. Honolka, P. Gambardella, L. Vitali, N. Abdurakhmanova, T.-C. Tseng, S. Rauschenbach, S. L. Tait, V. Sessi, S. Klyatskaya, M. Ruben and K. Kern, *J. Am. Chem. Soc*. 2010, **132**, 11900;

14 Z. Deng, S. Rauschenbach, S. Stepanow, S. Klyatskaya, M. Ruben and K. Kern, *Phys. Scr.* 2015, **90**, 098003.

15 (a) S. Thiele, F. Balestro, R. Ballou, S. Klyatskaya, M. Ruben, W. Wernsdorfer, *Science* 2014, **344**, 1135; (b) M. N. Leuenberger, D. Loss, *Nature* 2001, **410**, 789-793.

16 L. Margheriti, D. Chiappe, M. Mannini, P. E. Car, P. Sainctavit, M.-A. Arrio, F. B. de Mongeot, J. C. Cezar, F. M. Piras, A. Magnani, E. Otero, A. Caneschi, and R. Sessoli, *Adv. Mater*. 2010, **22**, 5488.

17 K. Katoh, Y. Yoshida, M. Yamashita, H. Miyasaka, B. K. Breedlove, T. Kajiwara, S. Takaishi, N. Ishikawa, H. Isshiki, Y. F. Zhang, T. Komeda, M. Yamagishi and Y. Takeya, *J. Am. Chem. Soc.* 2009, **131**, 9967.

18 L. Malavolti, M. Mattini, P.-E. Car, G. Campo, F, Pineider, R. Sessoli, *J. Mater. Chem. C*, 2013,**1**, 2935.

19 T. Komeda, H. Isshiki, J. Liu, Y. F. Zhang, N. A. S. Lorente, K. Katoh, B. K. Breedlove, M Yamashita, *Nat. Commun.* 2011, **2**, 217.

20 Y.-S. Fu, J. Schwöbel, S.-W. Hla, A. Dilullo, G. Hoffmann, S. Klyatskaya, M. Ruben, R. Wiesendanger, *Nano Lett.* 2012, **12**, 3931.

21 (a) T. Suzuki, M. Kurahashi, Y. Yamauchi, *J. Phys. Chem. B* 2002, **106**, 7643; (b) C. Wäckerlin, D. Chylarecka, A. Kleibert, K. Müller, C. Iacovita, F. Nolting, T. A. Jung, N. Ballav, *Nat. Commun.* 2010, **1**, 61; (c) S. Javaid, M. Bowen, S. Boukari, L. Joly, J. B. Beaufrand, X. Chen, Y. J. Dappe, F. Scheurer, J. P. Kappler, J. Arabski, W. Wulfhekel, M. Alouani, and E. Beaurepaire *Phys. Rev. Lett.* 2010, **105**, 077201; (d) H. Wende, M. Bernien, J. Luo, C. Sorg, N. Ponpandian, J. Kurde, J. Miguel, M. Piantek, X. Xu, P. Eckhold, W. Kuch, K. Baberschke, P. M. Panchmatia, B. Sanyal, P. M. Oppeneer, and O. Eriksson, *Nat. Mater*. 2007, **6**, 516.

22 M Gruber, F. Ibrahim, S. Boukari, H. Isshiki, L. Joly, M. Peter, M. Studniarek, V. D. Costa, H. Jabbar, V. Davesne, U. Halisdemir, J. Chen, J. Arabski, E. Otero, F. Choueikani, K. Chen, P. Ohresser, W. Wulfhekel, F. Scheurer, W. Weber, M. Alouani, E. Beaurepaire and M. Bowen, *Nat. Mater.* 2015, **14**, 981.

23 J. Schwöbel, Y. Fu, J. Brede, A. Dilullo, G. Hoffmann, S. Klyatskaya, M. Ruben, R. Wiesendanger, *Nat. Commun*. 2012, **3**, 953.

24 S. Sanvito *Nature Phys.* 2010, **6**, 562.

25 D. Klar, S. Klyatskaya, A. Candini, B. Krumme, K. Kummer, P. Ohresser, V. Corradini, V. de Renzi, R. Biagi, L. Joly, J.-P. Kappler, U. D. Pennino, M. Affronte, H. Wende, and M. Ruben *Beilstein J. Nanotechnol*. 2013, **4**, 320.

26 L. Malavolti, L. Poggini, L. Margheriti, D. Chiappe, P. Graziosi, B. Cortigiani, V. Lanzilotto, F. B. de Mongeot, P. Ohresser, E. Otero, F. Choueikani, Ph. Sainctavit, I. Bergenti, V. A. Dediu, M. Manninia, and R. Sessoli, *Chem. Commun*. 2013, **49**, 11506.

27 L. Malavolti, M. Mattini, P.-E. Car, G. Campo, F, Pineider, R. Sessoli, *J. Mater. Chem. C*, 2013,**1**, 2935.

28 A. L. Rizzini, C. Krull, T. Balashov, J. J. Kavich, A. Mugarza, P. S. Miedema, P. K.; Thakur, V. Sessi, S. Klyatskaya, M. Ruben, S. Stepanow, and P. Gambardella, *Phys. Rev. Lett.* 2011, **107**, 177205.

29 C. Nistor, C. Krull, A. Mugarza, S. Stepanow, C. Stamm, M. Soares, S. Klyatskaya, M. Ruben, Pietro Gambardella. *Phys. Rev. B* 2015, **92**, 184402.

30 A. L. Rizzini, C. Krull, T. Balashov, A. Mugarza, C. Nistor, F. Yakhou, V. Sessi, S. Klyatskaya, M. Ruben, S. Stepanow, P. Gambardella, *Nano Lett*. 2012, **12**, 5703.

31 S. Klyatskaya, J. R. G. Mascarós, L. Bogani, F. Hennrich, M. Kappes, W. Wernsdorfer, M. Ruben, *J. Am. Chem. Soc.* 2009, **131**, 15143.

32 a) M. Urdampilleta, S. Klyatskaya, M.–P. Cleuziou, M. Ruben, W. Wernsdorfer. *Nature Mater.* 2011, **10**, 502–506; b) M. Ganzhorn, S. Klyatskaya, M. Ruben, W. Wernsdorfer. *Nat. Nanotechnol.* 2013, **8**, 165; c) M. Urdampilleta, S. Klyatskaya, M. Ruben, W. Wernsdorfer. *Phys. Rev. B*. 2013, **87,** 195412; d) M. Ganzhorn, S. Klyatskaya, M. Ruben, W. Wernsdorfer. *Nat. Comms.,* 2016, **7**, 11443.

33 (a) W. Han, R. K. Kawakami, M. Gmitra, J. Fabian, *Nat. Nanotech*. 2014, **9**, 794; (b) O. Yazyev, M. Katsnelson, *Phys. Rev. Lett*. 2008, **100**, 047209.

34 (a) W. Kim, C. Li, F. A. Chaves, D. Jiménez, R. D. Rodriguez, J. Susoma, M. A. Fenner, H. Lipsanen, J. Riikonen, *Adv. Mater.* 2016, **28**, 1845; (b) Geim, A. K. *Science* 2009, **324**, 1530.

35 S. Jiang, S. Shi, X. Wang, *J. Phys. D: Appl. Phys*. 2014, **47**, 045104.

36 M. Lopes, A. Candini, M. Urdampilleta, A. Reserbat-Plantey, V. Bellini, S. Klyatskaya, L. Marty, M. Ruben, M. Affronte, W. Wernsdorfer and N, Bendiab, *ACS Nano* 2010, **4**, 7531.

37 A. Candini, S. Klyatskaya, M. Ruben, W. Wernsdorfer, M. Affronte, *Nano Lett*. 2011, **11**, 2634.

38 J. Gomez-Segura, I. Dıez-Perez, N. Ishikawa, M. Nakano, J. Veciana, D. Ruiz-Molina, *Chem. Commun*. 2006, 2866.

39 M. Gonidec, R. Biagi, V. Corradini, F. Moro, V. De Renzi, U. del Pennino, D. Summa, L. Muccioli, C. Zannoni, D. B. Amabilino, and J. Veciana, *J. Am. Chem. Soc.* 2011, **133**, 6603.

40 D. Klar, A. Candini, L. Joly, S. Klyatskaya, B. Krumme, P. Ohresser, J.-P. Kappler, M. Ruben, H. Wende, *Dalton Trans*. 2014, **43**, 10686.

41 M. Mannini, F. Bertani, C. Tudisco, L. Malavolti, L. Poggini, K. Misztal, D. Menozzi, A. Motta, E. Otero, P. Ohresser, P. Sainctavit, G. G. Condorelli, E. Dalcanale, and R. Sessoli, *Nat. Commun.* 2014, **5**, 4582.

42 C. Wäckerlin, F. Donati, A. Singha, R. Baltic, S. Rusponi, K. Diller, F. Patthey, M. Pivetta, Y. Lan, S. Klyatskaya, M. Ruben, H. Brune, and J. Dreiser, *Adv. Mater.* 2016, **28**, 5195.

43 (a) L. Ungur and L F. Chibotaru, *Inorg. Chem*. 2016, 10.1021/acs.inorgchem.6b01353; (b) N. F. Chilton, *Inorg. Chem*. 2015, **54**, 2097; (c) S. T. Liddle and J. v. Slageren, *Chem.Soc.Rev.,*2015,44,6655; (d) J. D. Rinehart and J. R. Long, *Chem. Sci*., 2011, **2**, 2078.

Dalton Transactions Accepted Manuscript

44 S. Marocchi, A. Candini, D. Klar, W. Van den Heuvel, H. Huang, F. Troiani, V. Corradini, R. Biagi, V. de Renzi, S. Klyatskaya, K. Kummer, N. B. Brookes, M. Ruben, H. Wende, U. del Pennino, A. Soncini, M. Affronte and V. Bellini *ACS Nano* 2016, accepted.

45 A. Candini, D. Klar, S. Marocchi, V. Corradini, R. Biagi, V. De Renzi1, U. del Pennino, F. Troiani, V. Bellini, S. Klyatskaya, M. Ruben, K. Kummer, N. B. Brookes, H. Huang, A. Soncini, H. Wende and M. Affronte, *Sci Rep.* 2016, **6**, 21740.

Table of Contents Image

Surface Confinement of TbPc₂-SMMs: Structural, Electronic and Magnetic Properties Eufemio Eufemio Moreno Pineda, Tadahiro Komeda, Keiichi Katoh, Masahiro Yamashitaand Mario Ruben

TbPc₂ crystal

Bulk material

Surface-confined TbPc₂ molecules

Planar surfaces
- metallic *vs.* non-metallic
- magnetic *vs.* non-magnetic
- ferro- *vs.* antiferromagnetic
- conducting *vs.* insulating

TbPc₂-based spintronic devices

Electrodes

The understanding of the SMM-surface interactions as well as the surfaces where the SMM are deposited is of upmost importance for the realisation of novel spintronic devices.